Contribution of the Zeeman effect to measured line profiles emitted by Alcator-C plasmas

R. D. Benjamin, J. L. Terry,* and H. W. Moos
Department of Physics and Astronomy, The Johns Hopkins University, Baltimore, Maryland 21218
(Received 11 June 1987)

The measured line profiles of the Si IV $3s\,^2S-3p\,^2P^\circ$ doublet during 10-T operation on the Alcator-C tokamak show evidence of a contribution due to the Zeeman effect to these profiles. The assumption that these line profiles are single lines broadened only by instrumental effects and thermal broadening yields apparent kinetic temperatures for the two lines which differ by approximately 50%. Neither of the resulting temperatures is reasonable for Si IV under typical Alcator operating conditions and the difference between the temperatures cannot be explained by Doppler effects. Modifying the nonlinear least-squares fitting routine to include the (unresolved) components predicted by the weak-field limit of the Zeeman effect yields kinetic temperatures for these lines which are in agreement and are reasonable for the region of the plasma in which Si IV exists. Finally, a study of the Zeeman effect in O VII shows that contributions from this process are important in determining ion temperatures from line broadening of the O VII $2s\,^3S_1-2p\,^3P_2^\circ$ emission line in the vuv spectrum from Alcator-C plasmas.

I. INTRODUCTION

Spectroscopic measurements of emission line profiles continue to be useful as a means of determining the ion temperature in tokamak plasmas. In order to be useful, however, interpretation of these measured line profiles must take into consideration all of the processes which may contribute to the line profile. In addition to the thermal broadening present in tokamak plasmas, it has been demonstrated that the Zeeman effect contributed to line profiles in visible emission spectra from Joint European Torus (JET) plasmas,[1] and the translational Stark effect has been observed in the Balmer lines of hydrogen.[2] In emission lines for which the fine structure is not resolved, both fine-structure splittings and the details of the l-shell populations of the levels involved in the transition may contribute to the measured line profile, especially for lines in the visible region of the spectrum resulting from charge exchange into excited states.[3] This paper discusses the contribution of the Zeeman effect to the measured vacuum ultraviolet (vuv) line profiles emitted from the high field ($B\sim 10$ T) Alcator-C (Ref. 4) tokamak plasma.

This paper is organized in the following manner. Section II describes the instrumentation used to make the measurements. It also presents the measured line profiles, and the fits to single lines, for the transitions of the Si IV $3s\,^2S-3p\,^2P^\circ$ doublet. Section III discusses the weak-field limit of the Zeeman effect and applies the results of this discussion to the lines of this Si IV doublet. Section IV discusses the Zeeman effect for the $1s2s\,^3S_1-1s2p\,^3P_2{}^\circ$ transition in O VII, a line routinely used for ion temperature diagnostics in the outer half of Alcator-C plasmas. Also presented are the results of an "exact" (i.e., valid for pure LS coupling) calculation of both the Zeeman splitting and relative line strengths of the Zeeman components for this transition, which confirm the applicability of the weak-field limit of the Zeeman effect to describe the contribution of this process to this line profile in Alcator-C plasmas.

II. INSTRUMENTATION

The measurements discussed in this paper were made using a high spectral resolution, photon counting detector[5] mounted at the exit plane of a 1-m Ebert-Fastie spectrometer. The spectrometer line of sight passes through Alcator C in a vertical direction, i.e., along a line of constant toroidal field strength. The spectrometer uses a plane grating with 3600 1/mm and exhibits a dispersion of ~ 2.9 Å/mm (~ 0.065 Å/pixel) in first order. The detector is an image intensifier, sensitive in the region from ~ 1150 Å to ~ 2000 Å, fiber optically coupled to a linear, self-scanning photodiode array. The geometric stability of this system (i.e., no moving parts), coupled with the high resolution (<50 μm) achievable with the photodiode array, makes this an excellent detector for line-shape studies.

The image intensifier contains three high strip current (~ 300 μA) microchannel plates (MCP's) in a "Z" configuration. The quantum efficiency of the detector has been enhanced by coating the surface of the first MCP with a film of CsI ~ 3000 Å thick. The output of the MCP stack is proximity focused onto a P-46 phosphor screen, which was deposited on the input face of the fiber optic bundle that serves as the output for the intensifier. This bundle is brought out of the vacuum chamber and a linear, self-scanning photodiode array is optically coupled to the external face. The modal gain of the intensifier is $\sim 3\times 10^7$ and the spot size of an amplified photoevent on the phosphor screen is ~ 350 μm (FWHM).

The photodiode array is a Reticon RL128SF,[6] containing 128 photodiodes with a slitlike geometry. Using

a scanning circuit designed for the authors,[7] the maximum pixel scanning frequency was determined to be approximately 4 MHz. Through the use of both pixel selection, i.e., reading data from less than the entire array, and the simultaneous scanning of both video lines of the photodiode array, frame times for the entire array of as little as 8 μs are possible, allowing frame rates in excess of 100 kHz. Even at these scanning frequencies, the pixel-to-pixel analog variability of the photodiode array in a flat field was less than 2% (i.e., the variability was at the level of the least significant bit of a seven-bit analog to digital converter).

The high spectral resolution exhibited by this detector is achieved by viewing the amplified output from each photoevent. The "center of gravity" of this output is calculated and is assumed to represent the location of the detected photon. This centroid is stored along with the frame number (i.e., the time of arrival of the photoevent) and is used to create a histogram which represents the spectrum seen by the detector. Examples of these histograms are shown in Fig. 1.

Figure 1 shows the single Gaussian fits to actual profiles, measured on the Alcator-*C* tokamak during 10-T operation, of the Si IV $3s\ ^2S-3p\ ^2P^\circ$ doublet. The fits

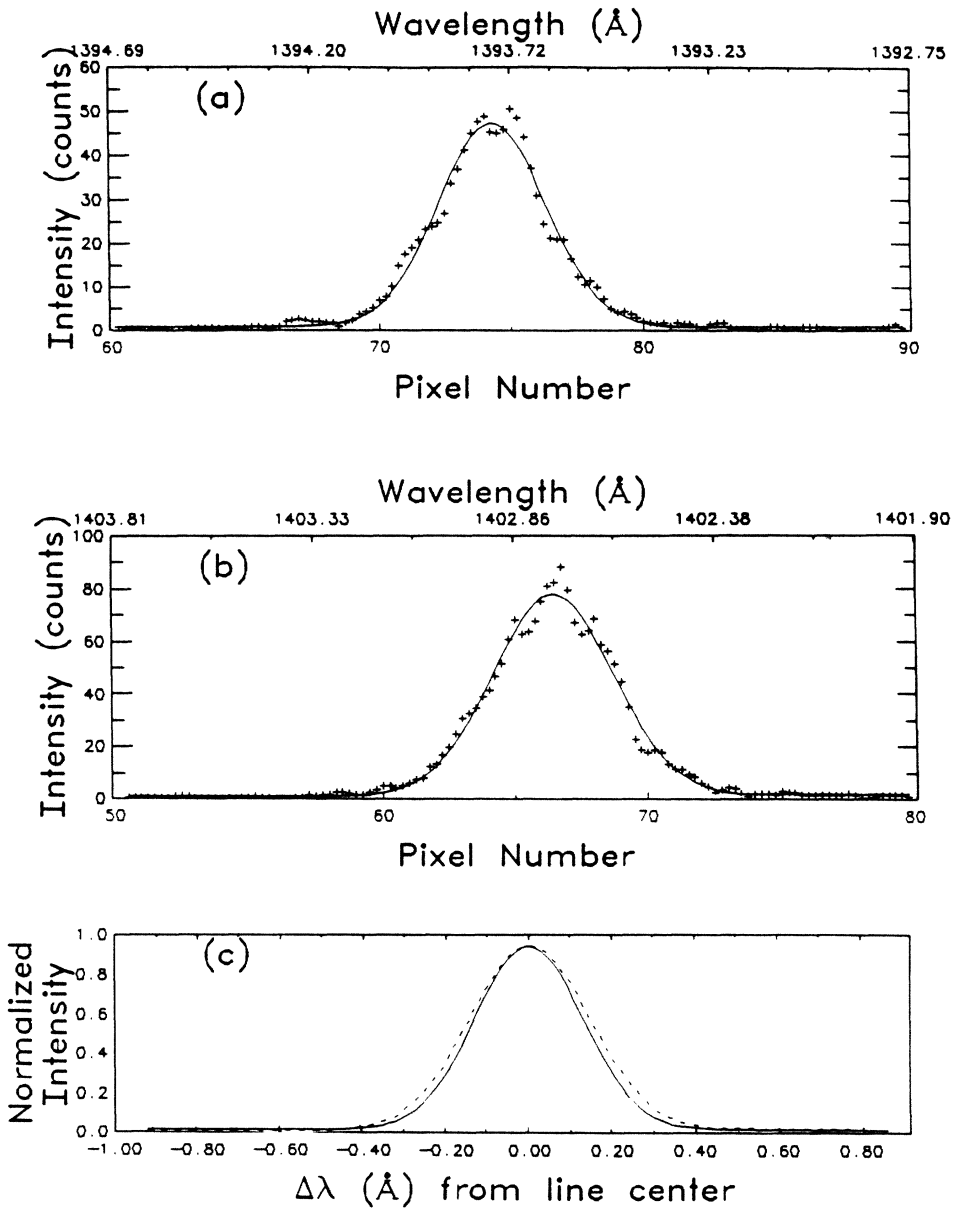

FIG. 1. (a) Single Gaussian fit to the Si IV $3s\ ^2S_{1/2}-3p\ ^2P^*_{3/2}$ line at 1393.8 Å during 10-T operation on Alcator *C*. The apparent kinetic temperature derived from the fit is $T_i = 155 \pm 13$ eV. (Each "pixel" is a "picture element" of the photodiode array.) (b) Single Gaussian fit to the Si IV $3s\ ^2S_{1/2}-3p\ ^2P^*_{1/2}$ line at 1402.8 Å during 10-T operation on Alcator *C*. The apparent kinetic temperature derived from the fit is $T_i = 220 \pm 13$ eV. (c) Fits from (a) (solid line) and (b) (dashed line), with their peak intensities normalized and plotted on same wavelength scale to demonstrate the difference in the widths of the lines.

to these lines, which are assumed to include only contributions from the instrumental profile and thermal broadening, yield linewidths which differ by $\sim 13\%$. Since the thermal contribution ($\Delta\lambda_T$) to the profile is determined by

$$(\Delta\lambda)^2=(\Delta\lambda_i)^2+(\Delta\lambda_T)^2 ,$$

where $\Delta\lambda$ is the full width at half maximum (FWHM) of the measured profile and $\Delta\lambda_i$ is the FWHM of the instrumental profile, this difference of 13% in the measured linewidths results in apparent kinetic temperatures which differ by $\sim 50\%$ (155 eV, derived from the line at 1393.8 Å, compared to 222 eV, derived from the line at 1402.8 Å). This difference in the widths of two lines emitted by the same ion, in this case Si IV, cannot be explained by Doppler shifts or broadening, since these processes would affect both lines in the same manner. Furthermore, Si IV exists in a narrow shell (~ 1 cm radial thickness) at the periphery ($r/a \sim 1$) of the Alcator-*C* plasma, and ion temperatures in the range from 150–230 eV in this region of the plasma are not supported by other diagnostics[8] or by computer modeling[9] of the plasma. Not included in the fits discussed above are the effects of Zeeman splitting of the lines, which could affect different lines from the same ion differently and which (as demonstrated below) are important in a high field machine such as Alcator *C*. In fact, evidence for contributions to the measured line profile due to the Zeeman effect has been seen in the visible region of the spectrum emitted by JET plasmas,[1] most notably using C II, Cr I, and Cl II lines. [JET is a much lower field machine ($B_\phi \sim 2$–3 T) than Alcator *C* ($B_\phi \sim 10$ T).]

III. FINE STRUCTURE AND THE WEAK-FIELD LIMIT OF THE ZEEMAN EFFECT

This section discusses the Zeeman effect on the fine structure of the Si IV $3s\,^2S-3p\,^2P^\circ$ doublet. The use of the weak-field limit of the Zeeman effect is justified if the ratio of $\mu_B B$ to the fine-structure splitting of the atom (ion) being studied is much less than 1. At field strengths typical of Alcator-*C* operation ($B \sim 10$ T), this ratio is ~ 0.01 for the Si IV $3p\,^2P^\circ$ term and the weak-field limit is a valid description of the interaction of this Si IV term with the Alcator-*C* magnetic field.

In the weak-field limit of the Zeeman effect, the shift of an energy level is calculated using first-order perturbation theory and is given by[10,11]

$$\Delta E=\langle \gamma LSJM \mid \mathcal{H}_{\rm mag} \mid \gamma LSJM \rangle , \tag{1}$$

where $\mathcal{H}_{\rm mag}$, the portion of the Hamiltonian describing the interaction with the magnetic field, is given by[10,11]

$$\mathcal{H}_{\rm mag}=-\bar{\mu}\cdot\mathbf{B} , \tag{2}$$

where $\bar{\mu}$ is the total magnetic moment of the electrons. $\bar{\mu}$ is defined in terms of the orbital and spin magnetic moments of the electrons as[11]

$$\bar{\mu}=-\left[\sum_i \mu_B \bar{l}_i+\sum_i g_s \mu_B \bar{s}_i\right] . \tag{3}$$

Substituting Eqs. (2) and (3) into Eq. (1) leads, after a minor amount of manipulation, to the well-known results for the weak-field limit of the Zeeman effect ($\mathbf{B}=B\hat{z}$) (Refs. 10 and 11):

$$\Delta E=g_J \mu_B B M , \tag{4}$$

where

$$g_J=\frac{J(J+1)+L(L+1)-S(S+1)}{2J(J+1)} +g_s\frac{J(J+1)-L(L+1)+S(S+1)}{2J(J+1)} . \tag{5}$$

From these calculated energy shifts and a knowledge of the selection rules for electric dipole transitions,[10,11]

$$\Delta M=0,\pm 1; M=0 \not\to M'=0 \quad \text{if } \Delta J=0 ,$$

the location of each component which results from the splitting of the levels due to the interaction with the magnetic field may be determined. It is then necessary to know the relative intensities of these components in order to calculate model spectra.

In the weak-field limit of the Zeeman effect, for observation perpendicular to the direction of the field, the relative intensities of the components[11] are, for π polarization [$\Delta M=0$ for electric dipole ($E1$) transitions],

$$S_\pi \propto |\langle \gamma' J' M \mid z \mid \gamma JM \rangle|^2 , \tag{6}$$

and for σ polarization ($\Delta M=\pm 1$ for $E1$ transitions),

$$S_\sigma \propto \tfrac{1}{2}|\langle \gamma' J' M\pm 1 \mid r_\pm \mid \gamma JM \rangle|^2 , \tag{7}$$

where

$$r_\pm=\mp(2)^{-1/2}(x\pm iy) . \tag{8}$$

Note that for magnetic dipole ($M1$) transitions, π polarization corresponds to $\Delta M=\pm 1$ and σ polarization to $\Delta M=0$.[10]

Using these results, the computer code which fits the line profiles was modified to perform a three-parameter fit to the sum of the Zeeman components which combine to form the measured profile. The three free parameters in the fitting procedure are the location of the center of gravity of the Zeeman components, the intensity of the strongest component, and the width of the individual components. (All of the components are forced to have the same width by the fitting routine.) The separation of the components is given by Eqs. (4) and (5) (since the magnitude of the magnetic field is known) and the relative intensities are determined by Eqs. (6) and (7).

The results of fitting the measured Si IV profiles using this code are shown in Fig. 2. The crosses represent the measured profiles, the solid upper line is the sum of the Zeeman components, and the lower solid lines represent the individual Zeeman components located at the positions predicted by the weak-field limit of the Zeeman

effect. The temperatures derived from the two lines of the doublet are now in agreement ($T_i = 63 \pm 5$ eV for the line at 1393.8 Å, $T_i = 69 \pm 4$ eV for the line at 1402.8 Å). Also, these temperatures are in far better agreement with those expected for the region of the plasma in which Si IV exists. Finally, note that the "goodness of fit" (determined by minimizing χ^2 in the nonlinear fitting routine) for this multicomponent fitting routine, which includes the unresolved Zeeman components, is not significantly better than that of the single-component fit, which ignores the Zeeman effect. Therefore, criteria other than just the goodness of fit must be used to determine if the functional form fit to the data is correct.

IV. THE ZEEMAN EFFECT IN O VII ($1s2s\ ^3S_1 - 1s2p\ ^3P_2^*$)

The evidence for the importance of the Zeeman effect in the line shapes of Si IV leads to the conclusion that care must be taken in deducing ion temperatures from the linewidths of other ultraviolet lines commonly used for this diagnostic purpose. A line routinely used for ion temperature measurements in the outer half of Alcator-*C* plasmas results from the $1s2s\ ^3S_1 - 1s2p\ ^3P_2^\circ$ transition in O VII (He-like). In order to illustrate the importance of Zeeman effect for this line, the prescription described in Sec. III is followed. The line profile is first fit by a single

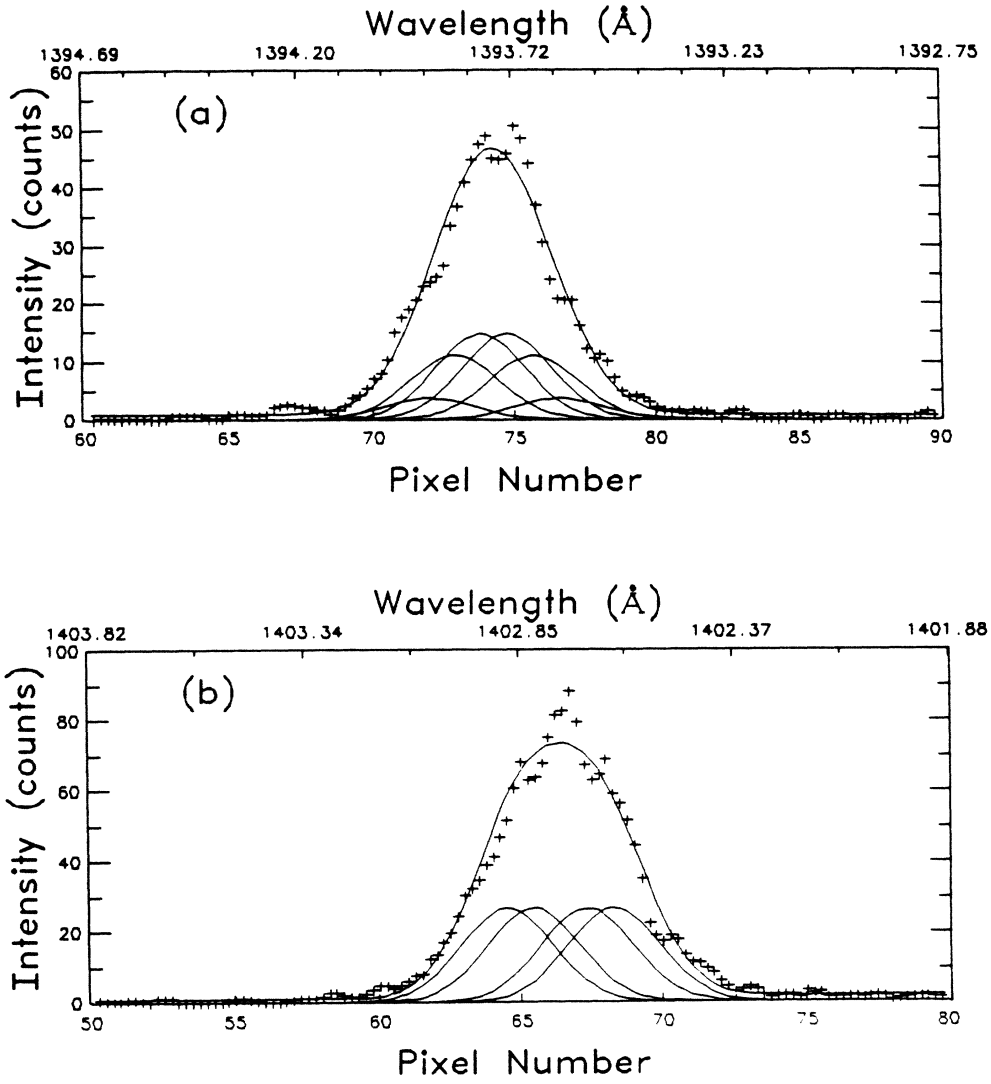

FIG. 2. (a) Measured profile (crosses), and the fit to the profile (upper solid line), for the Si IV line at 1393.8 Å using the fitting routine modified to account for the contribution to the line broadening due to the weak-field limit of the Zeeman effect. The lower solid lines are the individual Zeeman components located at the positions predicted by the weak-field limit of the Zeeman effect. The kinetic temperature derived from the fit is $T_i = 63 \pm 5$ eV. (b) Measured profile (crosses) and the fit to the profile (upper solid line) for the Si IV line at 1402.8 Å using the fitting routine modified to account for the contribution to the line broadening due to the weak-field limit of the Zeeman effect. The lower solid lines are the individual Zeeman components located at the positions predicted by the weak-field limit of the Zeeman effect. The kinetic temperature derived from the fit is $T_i = 69 \pm 4$ eV.

broadened line and an ion temperature deduced. Then the line is fit by assuming that it results from a sum of unresolved, individually broadened Zeeman components, whose splittings and relative intensities are known (since the field is known). The deduced ion temperatures are compared and, if different, the temperature based on the analysis which took into account the Zeeman effect is taken to be the correct one. (Note that this temperature will always be lower than the temperature resulting from the single line fit.) The results of the two analyses are shown in Fig. 3 for a discharge at 7.6 T, where the single line fit [Fig. 3(a)] yields a temperature of 321 ± 18 eV, and the multiZeeman component fit [Fig. 3(b), constructed in the same manner as Figs. 2(a) and 2(b)] yields the correct value of $T_i=274\pm15$ eV. Note that at 15 T, which the next generation of high-field tokamaks may reach, this effect will be larger.

Because of the importance of ion temperature measurements for magnetic confinement experiments, we have investigated quantitatively the accuracy of using the weak-field limit in evaluating the splittings and relative intensities of the Zeeman components of this O VII line. In particular, if purely LS coupled states are assumed, the magnitudes of both the splitting and the relative intensities can be calculated exactly for an arbitrary external magnetic field strength.[12] This calculation is based on the work of MacLean *et al.*,[13] which treats the same transition in C V (isoelectronic with O VII). The results are shown in Fig. 4. The shifts of the energy levels from their $B=0$ values, ΔE, scaled by $\mu_B B$ are given in

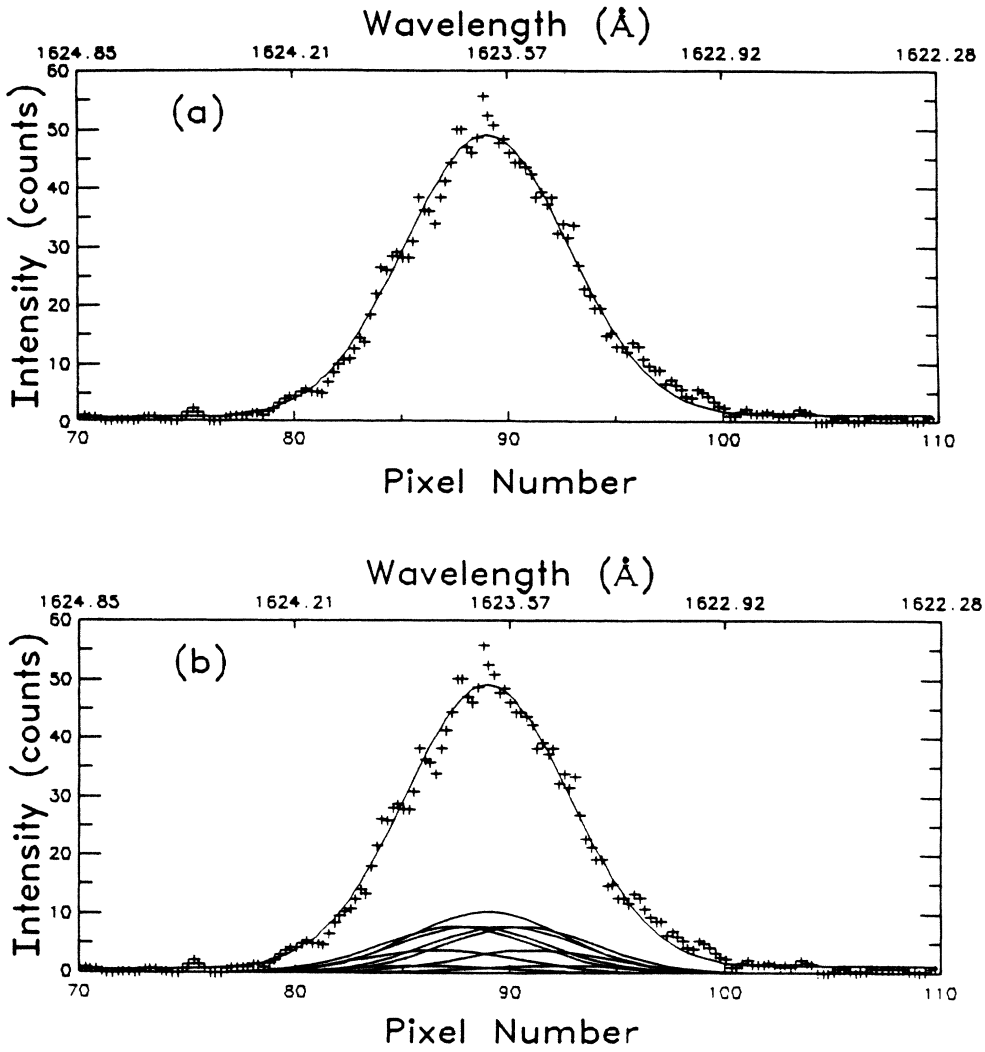

FIG. 3. (a) Single Gaussian fit to the O VII $1s2s\ ^3S_1-1s2p\ ^3P_2^*$ line at 1623.6 Å during 7.6-T operation on Alcator *C*. The apparent kinetic temperature derived from the fit is $T_i=321\pm18$ eV. (b) Measured profile (crosses) and the fit to the profile (upper solid line) for the O VII line at 1623.6 Å using the fitting routine modified to account for the contribution to the line broadening due to the weak-field limit of the Zeeman effect. The lower solid lines are the individual Zeeman components located at the positions predicted by the weak-field limit of the Zeeman effect. The kinetic temperature derived from the fit is $T_i=274\pm15$ eV.

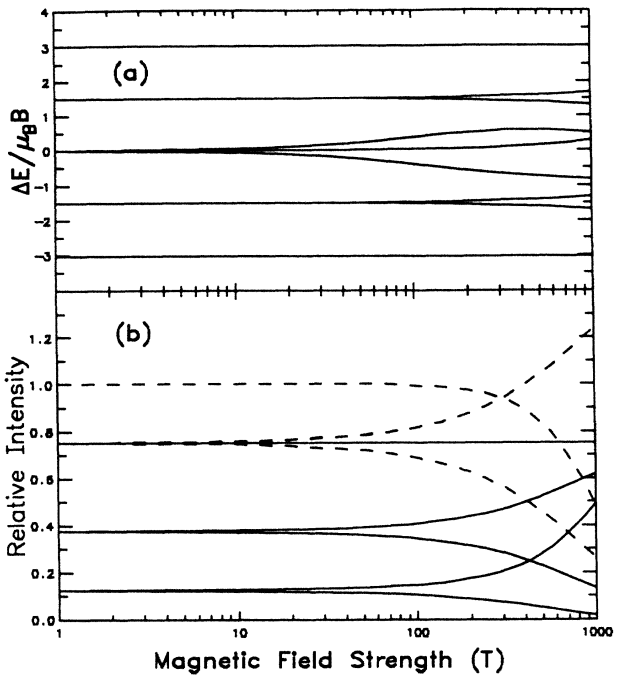

FIG. 4. (a) $[E_M^{J'}(B)-E_M^{J'}(B=0)]/\mu_B B$ as a function of the magnetic field strength for the $1s2p\ ^3P^\circ$ levels in O VII. (b) Relative intensities of the $1s2s\ ^3S_1-1s2p\ ^3P_2^\circ$ Zeeman components in O VII as a function of the field strength. π components are plotted using a dashed line; σ components are plotted using a solid line.

Fig. 4(a). (A horizontal line indicates $\Delta E \propto B$, i.e., the weak-field limit.) Figure 4(b) shows the relative intensities of the Zeeman components which split from the zero-field $1s2s\ ^3S_1-1s2p\ ^3P_2^\circ$ line (normalized so that the maximum of the $1s2s\ ^3S-1s2p\ ^3P_2^\circ$ intensities at zero field is 1). Again, any deviation from a horizontal line is indicative of deviation from the weak-field limit. Thus, in the range of magnetic field strengths over which Alcator *C* operates ($B \leq 12$ T), the results obtained using the weak-field limit are certainly adequate.

On the basis of this comparison and the fact that the ratio of $\mu_B B$ to the fine-structure splitting is less than 0.02 for all of the ions used for ion temperature measurements in this study, the weak-field limit of the Zeeman effect was deemed adequate to determine the contribution of this process to the measured line profiles in the vacuum ultraviolet region of the Alcator-*C* emission spectrum. It should be pointed out, however, that the "exact" treatment of the Zeeman effect may be necessary for lines in the visible emitted by low-*Z* ions (e.g., H, He, or Li). In any case, the influence of the Zeeman effect on the measured line profiles in the vuv in future generations of high-field tokamaks (Alcator *C*-Mod, CIT, etc.) cannot be neglected, especially in the outer regions of the plasma where the kinetic temperatures are low.

ACKNOWLEDGMENTS

The authors would like to thank the members of the Alcator scientific and technical staffs for their support and the opportunity to study these discharges. This work was supported by U.S. Department of Energy Grant No. DE-FG02-85ER53214-A000 at The Johns Hopkins University and U.S. Department of Energy Contract No. DE-AC02-78ET51013 at the Plasma Fusion Center.

*Present address: Plasma Fusion Center, Massachusetts Institute of Technology, Cambridge, MA 02139.

[1]P. G. Carolan, M. J. Forrest, N. J. Peacock, and D. L. Trotman, Plasma Phys. Controlled Fusion **27**, 1101 (1985).

[2]C. Breton, C. DeMichelis, M. Finkenthal, and M. Mattioli, J. Phys. B **13**, 1703 (1980).

[3]R. J. Fonck, D. S. Darrow, and K. P. Jaehnig, Phys. Rev. A **29**, 3288 (1984).

[4]S. Fairfax, A. Gondhalekar, R. Granetz, M. Greenwald, D. Gwinn, I. H. Hutchinson, S. E. Kissel, B. Lipschultz, E. S. Marmar, D. O. Overskei, D. S. Pappas, J. Parker, R. R. Parker, P. A. Pribyl, J. E. Rice, J. J. Schuss, N. Sharky, R. J. Temkin, J. L. Terry, R. Watterson, S. M. Wolfe, S. L. Allen, J. Castracane, and W. Hodge, in *Proceedings of the Eighth International Conference on Plasma Physics and Controlled Nuclear Fusion Research, Brussels, 1980* (International Atomic Energy Agency, Vienna, 1981), Vol. 1, p. 439.

[5]R. D. Benjamin, J. L. Terry, and H. W. Moos, Rev. Sci. Instrum. **58**, 520 (1987).

[6]EG&G Reticon, "*S*-Series Solid State Line Scanners 128, 512, and 1024 Elements," specification sheet (1978).

[7]Electronics designed by Spacom Electronics, Glen Arm, MD 21057.

[8]E. Lou, A. S. Wan, T. F. Yang, and B. Lipschultz, Bull. Am. Phys. Soc. **30**, 1497 (1985).

[9]S. M. Wolfe, C. Fiore, J. Terry, S. Knowlton, S. McDermott, J. Moody, M. Porkolab, and Y. Takase, Bull. Am. Phys. Soc. **31**, 1587 (1986).

[10]R. D. Cowan, *The Theory of Atomic Structure and Spectra,* Los Alamos Series in Basic and Applied Sciences (University of California Press, Berkeley, 1981).

[11]G. K. Woodgate, *Elementary Atomic Structure,* 2nd ed. (Oxford Science Publications, Oxford Press, Oxford, England, 1980).

[12]R. D. Benjamin, Ph. D. dissertation, The Johns Hopkins University, 1987 (unpublished).

[13]E. A. MacLean, J. A. Stamper, C. K. Manka, H. R. Griem, D. W. Droemer, and B. H. Ripin, Phys. Fluids **27**, 1327 (1984).